Published in "Geomorphology 290(): 101–113, 2017"
which should be cited to refer to this work.

New insights on permafrost genesis and conservation in talus slopes based on observations at Flüelapass, Eastern Switzerland

Robert Kenner[a,*], Marcia Phillips[a], Christian Hauck[b], Christin Hilbich[b], Christian Mulsow[c], Yves Bühler[a], Andreas Stoffel[a], Manfred Buchroithner[d]

[a] WSL Institute for Snow and Avalanche Research SLF, Davos, Switzerland
[b] Department of Geosciences University of Fribourg, Switzerland
[c] Institute of Photogrammetry and Remote Sensing, Dresden University of Technology, Germany
[d] Institute of Cartography, Dresden University of Technology, Germany

ARTICLE INFO

Keywords:
Ice rich permafrost
Snow cover
Rock glacier
Base of talus slopes

ABSTRACT

The talus slope at Flüelapass was the first mountain permafrost study site in Switzerland in the 1970s and the presence of ice-rich permafrost at the foot of the slope has been investigated in the context of several studies focusing on the role of snow cover distribution. We review previously developed hypotheses and present new ones using various data sources, such as temperature measurements in boreholes, a subaquatic DEM generated from unmanned aerial system (UAS) photogrammetry, terrestrial laser scan measurements of snow depth, geophysical ground investigations and automatic time-lapse photography. From this combination of data sources together with observations in the field, an interesting sequence of geomorphologic processes is established at Flüelapass. As a result we show how mass wasting processes can initiate the genesis and long-term conservation of ice-rich permafrost at the base of a talus slope.

1. Introduction

The lower fringe of mountain permafrost is often characterized by permafrost talus slopes or by rock glaciers with the root zone located in ice-rich permafrost talus slopes (Delaloye and Lambiel, 2005; Gruber and Haeberli, 2009; Lambiel and Pieracci, 2008). Permafrost in these landforms is, therefore, preferentially used to calibrate models of the local distribution of permafrost (Boeckli et al., 2012; Etzelmüller et al., 2001; Gruber and Hoelzle, 2001; Sattler et al., 2016) or to analyse the consequences of climate change on mountain permafrost (Monnier and Kinnard, 2016; Springman et al., 2012). The processes controlling the presence of permafrost in talus slopes, especially at elevations in the lower belt of the local permafrost environment are, thus, of particular interest. The talus slope at Flüelapass was the first site at which systematic research into mountain permafrost was carried out in the Swiss Alps and was first investigated by Haeberli (1975). Haeberli carried out extensive refraction surveys here and discovered the presence of ice-rich permafrost along the foot of the talus slope. This was later confirmed by vertical electrical soundings carried out by King et al. (1987). Furthermore, Haeberli (1975) showed a spatial correlation between thaw depth and perennial avalanche snow deposits: At the time of observation, the thaw depth was thinner at locations with perennial avalanche snow. This observed spatial relation led to the hypothesis that permafrost at the foot of talus slopes is present because of the insulating effect of superimposed perennial snow fields against radiation and atmospheric warming (Haeberli, 1975). We henceforth refer to this as the “insulation theory”. This was adopted by other studies carried out at Flüelapass. Lerjen et al. (2003) supplemented the hypothesis by adding the effect of soil properties (organic material vs. rock and gravel) on the thermal regime of the ground. Luetschg et al. (2004) analysed ground temperature simulations, ground surface and borehole temperature measurements and found that a delay in snow melt influences the active layer temperatures. This was interpreted as a confirmation of the insulation theory. Lerjen et al. (2003) and Luetschg et al. (2004) cited the effect of snow erosion by wind as a ground cooling factor in the Flüela talus slope but did not specifically show a spatial correlation between the distribution of permafrost and the spatial pattern of wind erosion.

Ice-rich permafrost often occurs at the foot of talus slopes (e.g. Lambiel and Pieracci, 2008; Scapozza et al., 2011). The insulation theory is one of two general explanations for this spatial niche of permafrost. The second explanation refers to air ventilation in talus slopes. Several studies have shown that ventilation can lead to substantial ground cooling in talus slopes and might contribute to

* Corresponding author.
E-mail address: kenner@slf.ch (R. Kenner).

permafrost conservation or development (Delaloye and Lambiel, 2005; Gądek, 2012; Morard et al., 2010; Niu et al., 2016; Schneider et al., 2012; Wicky and Hauck, 2016; Zacharda et al., 2007). On the basis of borehole temperature measurements Phillips et al. (2009) also demonstrated the occurrence of a ventilation effect underneath the perennially frozen part in the Flüela talus slope, but showed that it mostly causes positive temperatures in the voids in winter, thus contradicting a development of permafrost by ventilation at this site.

Snow coverage has changed at the Flüela site in recent decades: whereas perennial avalanche deposits at the base of the slope were the normal case in the 1970s according to Haeberli (1975), no perennial snow has occurred for the last 14 years at least, according to time-lapse images taken by an automatic camera. Data availability has significantly improved since the 1970s; e.g. borehole temperatures, geophysical soundings or remote sensing data and the length of observation periods have increased, allowing a critical verification of the hypotheses made in the past. It is still unclear whether a substantial effect of avalanche snow or wind driven snow redistribution occurs on the presence of ice-rich permafrost. Based on the improved dataset presented here, we will discuss whether the insulation theory is indeed the most relevant explanation for permafrost in the Flüelapass talus slope and present an alternative hypothesis which may be relevant for other sites with ice-bearing talus slopes. A key question here: what is the origin of the excess ice in the Flüela talus slope?

2. Site description and geomorphological history

The talus slope at Flüelapass is located on the NE flank and at the base of the summital rock wall of "Chlein Schwarzhorn", a 2986 m high peak in the eastern Swiss Alps (46°44′37.804″N 9°56′13.758″E). The foot of the talus slope at 2375 m a.s.l. forms the eastern shore of lake Schottensee, which has an area of 83,000m^2 (Fig. 1). Two 20 m vertical boreholes were drilled in the slope in 2001; the upper one (B1) is 125 m above the lake at 2501 m a.s.l., and the lower one (B2) is 20 m above the lake at 2394 m a.s.l. Around B1 the slope is covered with soil and grass and positive temperatures are registered throughout the borehole (no permafrost), whereas the foot of the slope around B2 is devoid of vegetation, covered in talus and has negative temperatures between 3 and 10 m depth (permafrost). The stratigraphies of both boreholes are presented in Phillips et al. (2009) and apart from the surface and the ice content they are very similar, with rocks and gravel and a very blocky layer that is a few metres thick around 10 m (B1) and 15 m (B2) depth, respectively. The grain sizes of the talus at the surface of B2 range between 10 and 40 cm. The lower quarter of the slope is a snow avalanche deposit zone and avalanche snow often persists here for long periods of the summer.

A series of interesting landforms at Flüelapass reveal the history of the site and help to elucidate the genesis of permafrost ice at the bottom of the talus slope. These landforms are highlighted on the orthophoto in Fig. 2. There is a conspicuous shallow channel around B2, delimited by two sharply defined parallel escarpments. These escarpments are oriented parallel to the slope and reach from the lower third of the talus slope to the lake shore. We have observed similar channels with sharply defined escarpments in talus slopes at other sites. Fig. 3 shows a similar feature at a talus slope at Piz Corvatsch (Eastern Swiss Alps), close to the Murtèl rock glacier (Haeberli et al., 1998). A distinct lobe is evident directly below the shallow channel at Piz Corvatsch. Unpublished terrestrial laser scanning (TLS) and electric resistivity tomography (ERT) measurements we carried out indicate that the Corvatsch lobe is creeping downslope and contains ice. It is, therefore, very likely that the loose rock material forming the lobe originates from the shallow channel above and was displaced by permafrost creep.

At Flüelapass a similar lobate form is also evident below the shallow channel, at the lake bottom. The orthophoto in Fig. 4, acquired by UAS borne photogrammetry shows this lobe, which encloses a deep depression in the lake. Based on the morphology (Haeberli, 1985) we consider both lobate features at Piz Corvatsch and Flüelapass as being small rock glaciers.

Rock glaciers cannot form under water, as the water temperature would lead to ice melt (Haeberli et al., 2001). The only explanation for the underwater rock glacier at Flüelapass is, therefore, that the lake is younger than the rock glacier. This in turn explains the deep depression in the underwater lobe. After the lake flooded the rock glacier, the ground ice melted and a thermokarst depression developed. The rock glacier front and side walls which contained less or no ice now form the underwater lobe with 45° steep side walls (Fig. 5). Similar features are visible all along the SW lakeshore, indicating widespread permafrost creep at the base of the talus slope in the past (Figs. 2 and 4). The sizes and positions of the lobes correspond to the main deposition areas of snow avalanches.

At the NW end of the lake there is a field of large rocks and boulders with a distinctly rougher texture than the neighbouring talus slopes (Fig. 2). This area is clearly the deposition zone of a large rock fall originating from the rock wall NW of the lake. This deposit likely

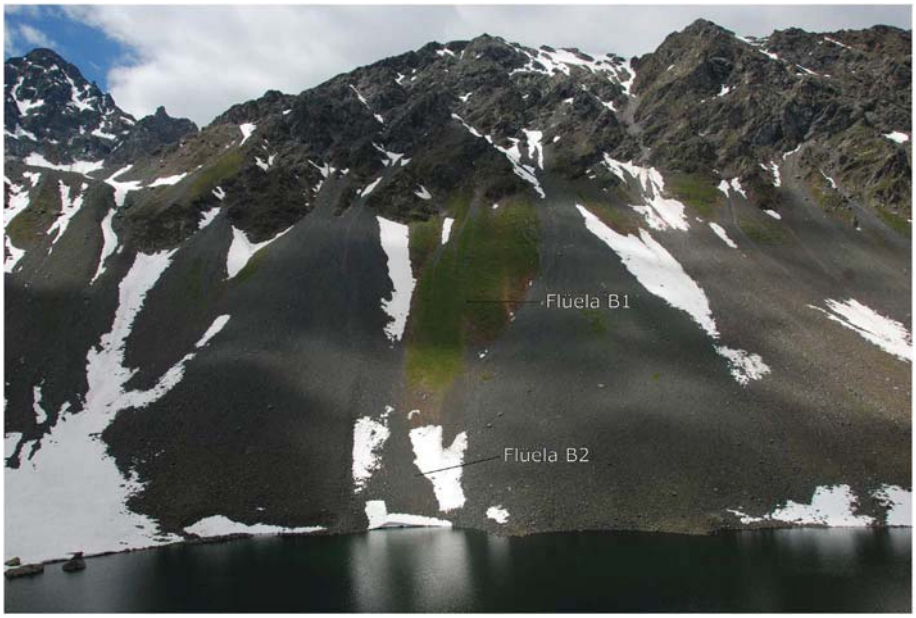

Fig. 1. Photograph showing the Flüela talus slope on 13.07.2009 with the positions of the two boreholes. The pattern of snow melt out is quite complex (Photograph: M. Phillips).

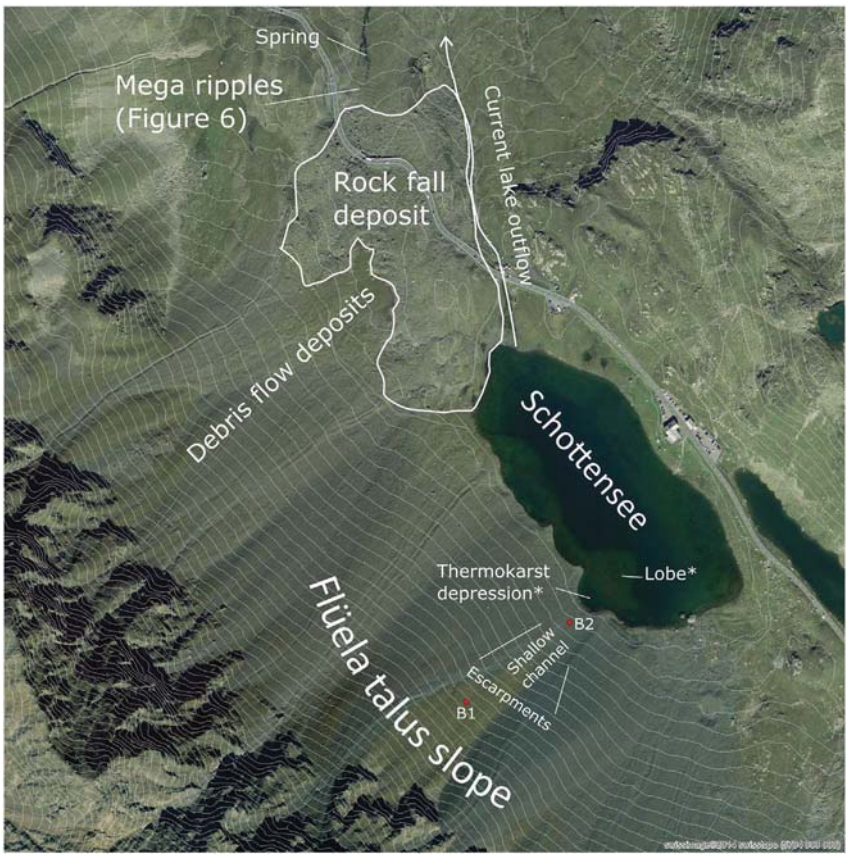

Fig. 2. Orthophoto of the Flüelapass site with mapped landforms. Each of these features is discussed in the study (orthofoto: swissimage©2014 swisstopo (5704 000000).

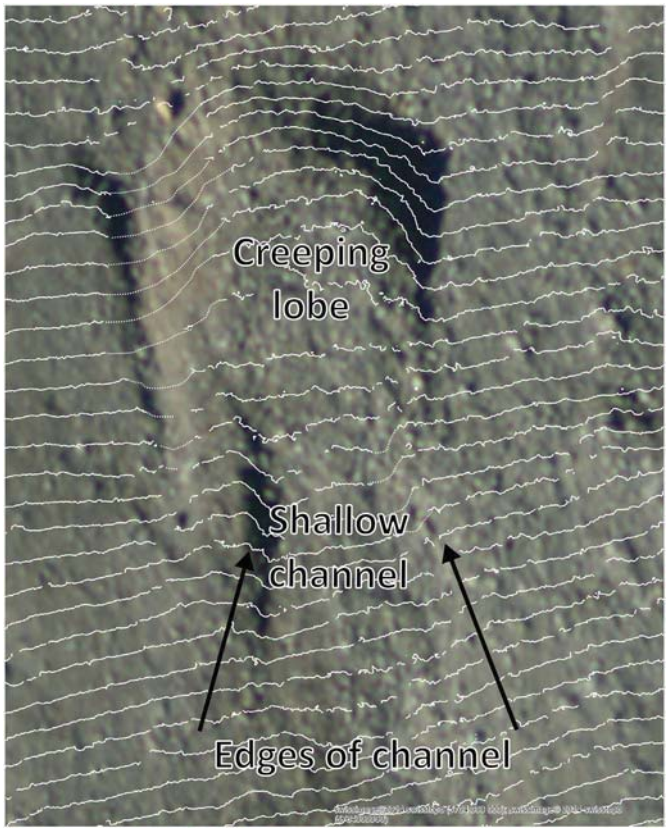

Fig. 3. Example of a creep lobe at Piz Corvatsch, which is similar to that at Flüelapass (orthofoto: swissimage©2014 swisstopo (5704 000000).

blocked the northward runoff from Flüelapass and dammed the lake (Suchlandt and Schmassmann, 1936) which then flooded the rock glacier. At the Eastern side of the rock fall deposit a new stream channel has developed (Fig. 2). A part of the lake runoff is however still discharged under the rock fall deposit and is released by a spring at the N lower end of the rock fall deposit. Directly around and below the spring, a series of ripple-like features are evident with a wave length of approximately 6 m (Fig. 6). These are probably mega-ripples, which are formed by flood waves released during a lake outburst (Burr et al., 2009). Hence, rock fall event(s) and the subsequent lake formation were probably followed by a partial lake outburst here. Similar ripples are also known to be formed by permafrost creep (Frehner et al., 2015). Other geomorphologic characteristics of a relict rock glacier are however missing here.

3. Methods

3.1. Temperatures in boreholes

The boreholes at Flüelapass were equipped with thermistor chains (with 12 YSI 44008 thermistors) and a Campbell CR10X data logger. Temperatures are measured every 2 hours at 0.25, 0.5, 1.0, 1.5, 2.0, 3.0, 4.0, 6.0, 8.0, 10.0, 15.0 and 20.0 m depth. In February 2016 the thermistor chain was removed from B2 for recalibration and it was found that the thermistors at 6.0, 8.0, 10.0 and 15.0 m depth had been subject to a slow but distinct temperature drift (causing artificially high temperatures to be registered). This problem can be induced by moisture in the thermistors and tends to start slowly and increase exponentially (Luethi and Phillips, 2016). Recalibration of this thermistor chain and measurements made from July 2016 onwards with a new thermistor chain indicate that the drift was such that the postulation made by Phillips et al. (2009) regarding the occurrence of permafrost degradation from the base upwards is likely wrong and that

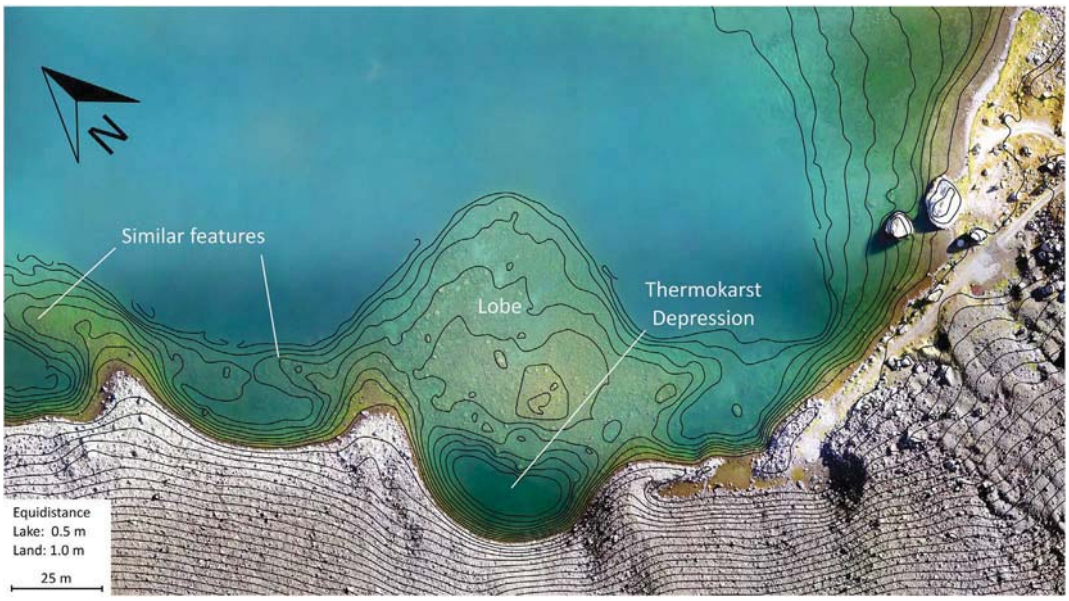

Fig. 4. Orthophoto created from UAS imagery with the contour lines of the corresponding (subaquatic) DEM. The underwater lobe constitutes the front of a relict rock glacier with a deep thermokarst sink in its centre (Photograph SLF UAS, 2016). Similar features are visible along the lake shore.

Fig. 5. The steep front of the flooded rock glacier at the foot of the Flüela talus slope. (Photograph: M. Schaer, 08.10.2012).

the ground ice is still intact to a depth of approximately 10 m. It is difficult to determine the exact time at which drift started.

Borehole temperatures are used to define the thickness of permafrost and active layer (AL). Furthermore, we calculated thermal orbits by plotting temperatures of neighbouring thermistors against each other. The shape of these orbits gives indications on the type of heat transfer occurring (Beltrami, 1996; Smerdon et al., 2009; Zenklusen Mutter and Phillips, 2012b). The end of snow melt dates are defined by the date at which the spring zero curtain ends at 0.25 m depth. We defined the maximal thickness of the AL by linear interpolation between the lowest thermistor in the AL and the uppermost thermistor in the permafrost. Linear interpolation might not be appropriate to find the absolute thickness of the AL but gives an indication of the variability of AL thickness over time.

3.2. Geophysics

In addition to early refraction seismic surveys (Haeberli, 1975) and vertical electrical soundings (King et al., 1987) at the Flüela talus slope, new geophysical surveys were conducted in summer 2009 with the aim to map the spatial distribution of ground ice in the talus slope in more detail. We used electrical resistivity tomography (ERT) and refraction seismic tomography (RST), as both methods are highly sensitive to the transition from unfrozen to frozen materials and, thus, well suited to identify ice-rich permafrost (e.g. Kneisel and Schwindt, 2008).

ERT data were obtained along a vertical profile that crossed both borehole positions and three parallel horizontal profiles in the lower part of the talus slope. The measurements were carried out using a *Geotom* multi-electrode instrument (Geolog) and 75 electrodes with 4 m spacing (resulting in 296 m profile lines). Measurements were performed in the Wenner-Schlumberger configuration, as a good compro-

Fig. 6. Mega-ripples around the spring below the rock fall deposit at Flüelapass, which may have been formed by a lake outburst after the rock fall which dammed the lake. (Photograph: R. Kenner, 28.09.2016).

mise between spatial resolution and high signal-to-noise ratio. Data processing was conducted with filtering procedures and choice of inversion parameters as detailed e.g. in Hilbich et al. (2011). Data inversion (i.e. the calculation of the specific resistivity model of the subsurface based on the measured apparent resistivities) was performed using the Software *Res2DInv* (Loke 2012).

In addition, RST data were collected parallel to selected ERT profiles, but with smaller extent and penetration depth (see Fig. A, Appendix). We used a 24 channel *Geode* instrument (Geometrics) with a sensor spacing of either 4 or 5 m (resulting in 92 and 115 m profile lines) and shot points every 8 or 10 m, respectively. Tomographic inversion was performed using the software ReflexW (Sandmeier, 2014). First arrival picking and choice of inversion parameters were conducted as described in Hilbich (2010).

Although the RST method often reveals less detailed structural information of the subsurface, it provides valuable complementary data in ambiguous situations (e.g. Hilbich 2010). Especially in talus slopes (or other coarse blocky landforms) resistive anomalies can usually be interpreted as zones with high porosity, but it cannot always be determined whether they are predominantly air- or ice-filled voids. In contrast, seismic velocities of air and ice differ by one order of magnitude and ice-rich anomalies can usually be well distinguished from zones with air-filled voids (Hauck and Kneisel, 2008; Kneisel and Hauck, 2003; Kneisel and Schwindt, 2008).

3.3. Subaquatic digital elevation model from UAS borne photogrammetry

A digital elevation model (DEM) and an orthophoto of the base of the talus slope and of parts of the lake bottom were calculated from aerial images acquired with a Sony NEX-7 camera (24 Mp, 20 mm F/2.8 optical lens), mounted on an Ascending Technologies (AscTec) Falcon 8 octocopter (Bühler et al., 2016). We obtained a DEM resolution of 4 cm and an orthophoto resolution of 2 cm. The images were taken on 08.09.2016 from around 100 m above ground with an overlap of approximately 75% along track and 65% across track. Eight ground control points were integrated in the set of images, whose coordinates were defined using a Topcon GR5 GNSS receiver in real time kinematic mode. For image orthorectification and the generation of a georeferenced 3D point cloud of the ground surface the Agisoft software PhotoScan Pro v1.2.6 was used. Additionally we carried out point reference measurements of the water depth, using a sounding pole and the Topcon GR5 GNSS receiver.

When comparing the reference depth measurement with the 3D-data derived from aerial images, the effects of optical refraction on the water surface are quite prominent (Rinner, 1969). This leads to an underestimation of water depth, because the image ray path is assumed to be a straight line in PhotoScan, which is only valid for land-points. In our case, the differences reached values from ~0.3 m for water depths of about 1.3 m up to ~0.8 m for depths of 2.8 m. This means that the refraction has to be considered for subaquatic points. Unfortunately, most commercial software cannot provide this function. Therefore a special software was developed at the Institute for Photogrammetry and Remote Sensing at TU-Dresden (Mulsow, 2010) for the processing.

The results from PhotoScan were used as initial values for image orientation, camera calibration data and the DEM. New image points were automatically measured in the photographs and classified as subaquatic or land-points. The water surface was modelled as a plane, with its height determined from the GNSS measurements and its surface normal in vertical direction. For the refraction index of water, a tabular value of 1.33 was assumed. Finally, the data were processed simultaneously in a bundle-adjustment to calculate the image orientation, the camera calibration data as well as the surface points. In contrast to a standard bundle adjustment, our software was extended with a multi-media-module. In the standard pinhole camera model the image ray path is defined as a straight line between the object point, the projection centre of the camera and the image point. In the case of a subaquatic point, the ray path is a polygon between an object point, the penetration point through the water, the projection centre and the image point. The implemented multimedia-module calculates the refraction at the interface between water and air and provides the image ray direction between the image point and the projection centre for the bundle adjustment. For land-points the direction is given by the vector between the projection centre and the point itself. In the case of a subaquatic point it is given by the projection centre and the penetration point of the image ray through the water surface. A detailed description can be found in (Mulsow, 2010). When comparing the photogrammetrically derived DEM with reference lake depth measurements, an RMS of 10 cm could be obtained (9 check points). This corresponds to the relative accuracy of the subaquatic reference points, obtained from the adjustment (9 cm).

3.4. Terrestrial laser scanning

Terrestrial laser scans were carried out yearly in summer between 2009 and 2016 to capture potential surface deformations and to obtain a detailed DEM of the Flüela talus slope. An additional scan was carried out on 23.01.2013 to determine the distribution of snow depth over the talus slope. The laser scans were performed using a Riegl VZ6000 long range laser scanner. The point clouds showed a spatial resolution of 10 cm and were georeferenced by control points (Kenner et al., 2014). The co-registration of the scans was verified in snow free areas like rock walls or on boulders.

3.5. Time-lapse camera

A time-lapse camera (Panasonic Lumix DMC FZ100) is located on a small rock wall opposite the talus slope. It takes photographs of the lake and of the talus slope on a two-hourly basis from 06.00 am until 22.00 pm. The pictures allow the distribution of snow cover and avalanche activity to be determined.

4. Results

4.1. Ground temperatures in the Flüela boreholes

The ground temperatures measured in B2 from 2002 to 2016 are shown in Fig. 7. The rectangle marks the artefact caused by thermistor drift between 6 and 10 m depth which falsely indicates permafrost thaw. These depths were excluded from the analysis. The thickness of the AL is constant over the whole time series and is shown in Table 1, together with the end of snow melt dates. The stable ground ice conditions are also indicated by the TLS measurements which show no signs of ground deformation. The dates of snow disappearance, deduced from the uppermost borehole temperatures, are confirmed by the snow melt progression visible in the time-lapse images. The permafrost is warm with maximum temperatures around − 0.1 °C at all depths. The thermal orbits of the thermistors at 15 m and 20 m depth (Fig. 8, top) are chaotic and indicate the ventilation analysed by Phillips et al. (2009). The seasonal thermal effect of ventilation underneath the permafrost is also clearly visible in Fig. 7. It causes a cooling of the ground below the permafrost body and, thus, probably influences the lower border of the permafrost. However as the temperatures are mostly positive throughout the year in the ventilation zone, they are too high to cause the presence of permafrost on their own. The thermal orbits of the thermistors at 3 m and 4 m depth, both located in permafrost, show ellipsoidal shapes and indicate the dominance of conductive heat transfer initiated from the top (Fig. 8, bottom). In contrast, in borehole B1 positive temperatures are recorded at all depths throughout the year. Only the thermistor at 0.25 m depth measured slightly negative temperatures during a few winters.

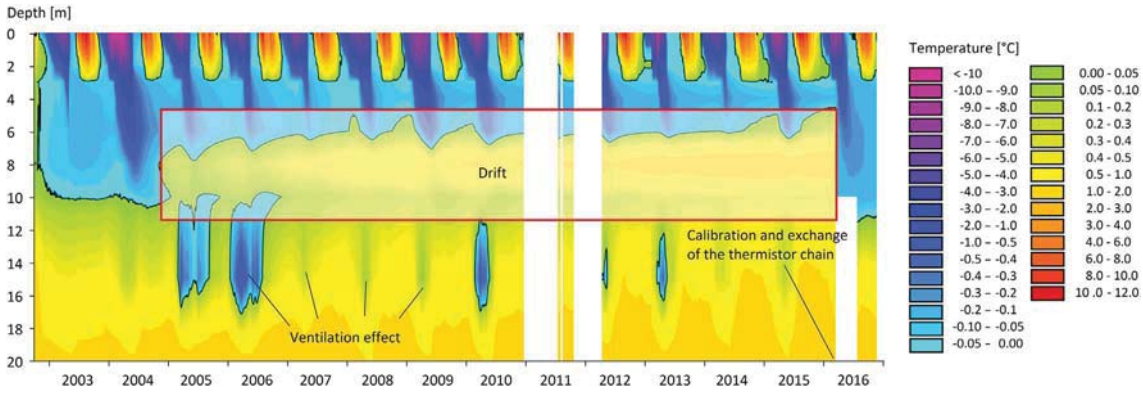

Fig. 7. Contour plot of the borehole temperature time series in B2. Some thermistors were subject to thermal drift. In spring 2016 the thermistor chain was exchanged and the new data reveal that no change in permafrost extent occurred since the beginning of the time series.
(Data: SLF/PERMOS).

Table 1
End of spring zero curtain at 0.25 m depth (date of end of snow melt) and maximum active layer thickness at B2.

	End of spring zero curtain at 0.25 m depth	Active layer thickness
2003	12.06.	2.96
2004	17.07.	2.90
2005	28.06.	2.93
2006	26.06.	2.96
2007	03.06.	2.97
2008	24.06.	2.96
2009	03.07.	2.95
2010	02.07.	2.96
2012	29.06.	2.96
2013	22.07.	2.95
2014	17.06.	2.96
2015	13.06.	2.96

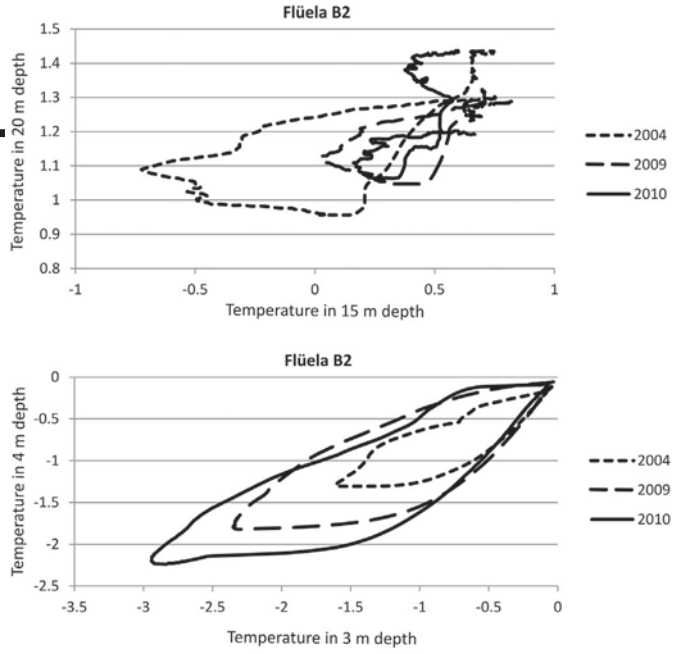

Fig. 8. Thermal orbits of neighbouring thermistors in the borehole B2. Elliptic orbits indicate purely conductive heat transfer.
(Data: SLF/PERMOS).

4.2. Geophysics

In accordance with the results of the earlier seismic refraction soundings (Haeberli, 1975) and vertical electrical soundings (King et al., 1987), our ERT data indicate ice-rich permafrost at the base of the talus slope, which slowly thins out upslope (Fig. 9). This interpretation is also supported by our refraction seismic data, which show high P-wave velocities in this area indicating ground ice occurrence as opposed to air-filled voids, which would lead to lower P-wave velocities (Fig. A, Appendix). Three horizontal ERT profiles (Fig. 9; Fig. A, Appendix) indicate that the ice rich permafrost is present all along the lake shore. Further upslope, in the central part of the longitudinal profile, a layer with high resistivities (10000–20,000 Ωm) is visible at 10–30 m depth, which can be interpreted as a blocky substrate with high air- or low to moderate ice content. Bedrock was detected at approximately 30–40 m depth in the central part of the profile and at 15 m depth at borehole B1 (Fig. 9). In general, our results largely confirm the findings of Haeberli (1975) and King et al. (1987), partly with a remarkable correspondence, given the differences in measurement geometry, acquisition parameters and data processing. This relates especially to the spatial extent of the confined ice-rich permafrost body at the foot of the talus slope.

4.3. Subaquatic DEM

The orthophoto and the correspondent DEM acquired using unmanned aerial system UAS photogrammetry is shown in Fig. 4. The elevation model shows that the thermokarst depression is approximately 4.5 m deep in relation to the surrounding lobe. The absolute water depth in the depression is approximately 7 m at a distance of 11 m from the shore and the highest point of the lobe is 0.5 m under water at a distance of 33 m from the shore.

5. Interpretation and discussion

5.1. The genesis of excess ice permafrost in the Flüela talus slope

The geomorphological analysis of the Flüela site indicates the former occurrence of permafrost creep in the talus slope. This process is caused by excess ice (Arenson et al., 2002; Haeberli et al., 2006; Kääb and Reichmuth, 2005). The presence of excess ice at the foot of the talus slope indicates a possibly important if not dominant process of ground ice formation: the burial and/or embedding of (avalanche) snow deposits below steep rock walls or talus slopes by rock fall or scree slides (Humlum et al., 2007; Isaksen et al., 2000; Kenner and Magnusson, 2017; Potter, 1972). Sanders et al. (2014) presented a case study of such a rock fall on snow, directly above a relict rock glacier. At the Flüela site the avalanche snow deposits easily reach 7 m thickness.

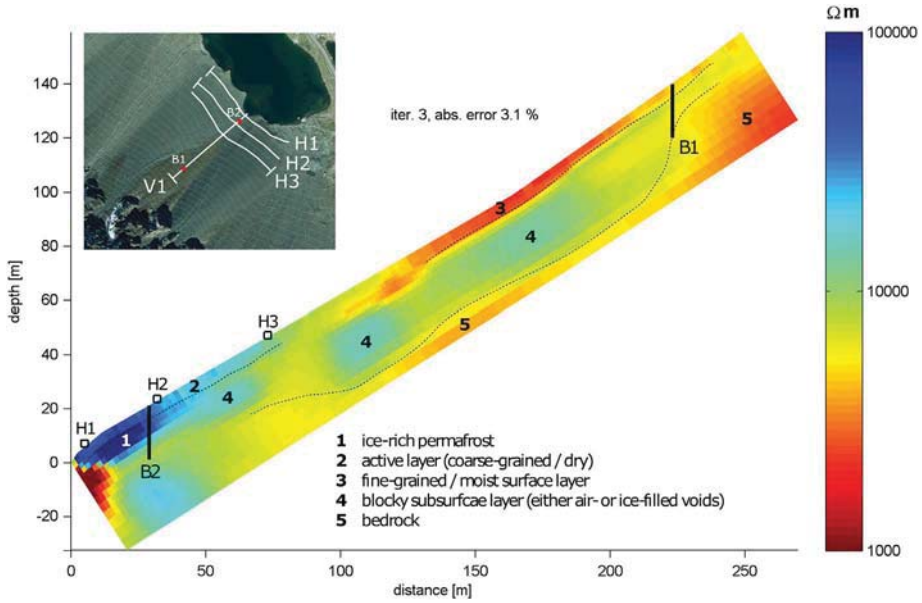

Fig. 9. Electrical resistivity tomography profile of the Flüela talus slope. The white line in the orthophoto indicates the position of the profile. The positions of 3 supplementary cross section profiles, included in the appendix, are mapped with grey lines. The red circles mark the positions of the boreholes. The high resistivity values in the lower part of the talus slope indicate ice rich ground.

Fig. 10. Avalanche deposit interspersed with scree around the Borehole B2. (Photograph: M. Phillips, 02.03.2017).

Table 2
Percentage of 122 rock glaciers in the Albula Range with avalanche snow deposits in the root zone in autumn or late summer.

Date	27.08.2015	19.08.2012	20.08.2009	09.09.2006
Percentage of rock glaciers with avalanche snow in root zone	63%	80%	84%	57%

Thin debris layers of a couple of cm can already delay the melt of such snow deposits (Evatt et al., 2015; Nicholson and Benn, 2006; Reznichenko et al., 2010). Thus, in addition to one large rock fall, a sequence of smaller events would suffice to effectively insulate snow remains. Another means of debris layer formation on avalanche snow can be the melt out of scree, which is incorporated in the avalanche snow. Fig. 10 shows an avalanche deposit at B2 in March 2017 which is interspersed with scree. In case of multiple perennial avalanche layers, the scree can form a closed layer at the surface due to melt out. This activates a positive feedback, as firn melt is reduced by the scree, thus enabling scree accumulation on top of the firn for a longer period of time.

During the last glaciation, the maximal ice coverage reached approximately 2600 m a.s.l. at Flüelapass, as is demonstrated by the presence of polished rocks to this elevation E of the lake. In its present form, the investigated talus slope must, therefore, have developed postglacially (Phillips et al., 2009). The formation of talus slopes like the one at Flüelapass would, however, not have been possible during the Holocene, taking current rates of erosion as a reference (Ballantyne, 2002). Instead, rock fall activity was generally much more intense at the beginning of the Holocene than today (e.g. Haeberli et al., 1999). This might mainly have been caused by the strong warming (Fischer et al., 2006; Gruber and Haeberli, 2007; Noetzli et al., 2003) after the last glaciation. During periods with frequent rock fall during which the talus slope developed, the burial of avalanche snow, leading to ground ice formation is likely (Phillips et al., 2009) and explains the correlation of avalanche depositions and subaquatic creep lobes in terms of their size and position.

There are some other indications for the relevance of excess ice formation because of the burial of avalanche snow in alpine permafrost in general. Kenner and Magnusson (2017) highlighted these processes by analysing an inventory of rock glaciers in the Swiss Albula mountain range. We have since analysed the avalanche snow coverage of all 122 rock glaciers in this inventory: Aerial images taken in four different years between 2006 and 2015 were analysed to define the number of talus slopes in the root zone of rock glaciers covered with avalanche snow (Table 2). On average, 71% of the rock glaciers still had snow in the root zones at the time of image acquisition in autumn or late summer. Rock fall can, therefore, potentially cover avalanche snow at these locations at any time of year. Furthermore snow avalanche deposits are limited to slope angles below 30° because avalanches do not stop in steeper slopes (Munter, 2003). The same slope limitation is valid for ice rich permafrost (Kenner and Magnusson, 2017), which applies to the Flüela talus slope but also for example to the talus slopes investigated by Lambiel and Pieracci (2008). Fig. B (Appendix) shows the zones of high electrical resistivity (indicative for ice-rich perma-

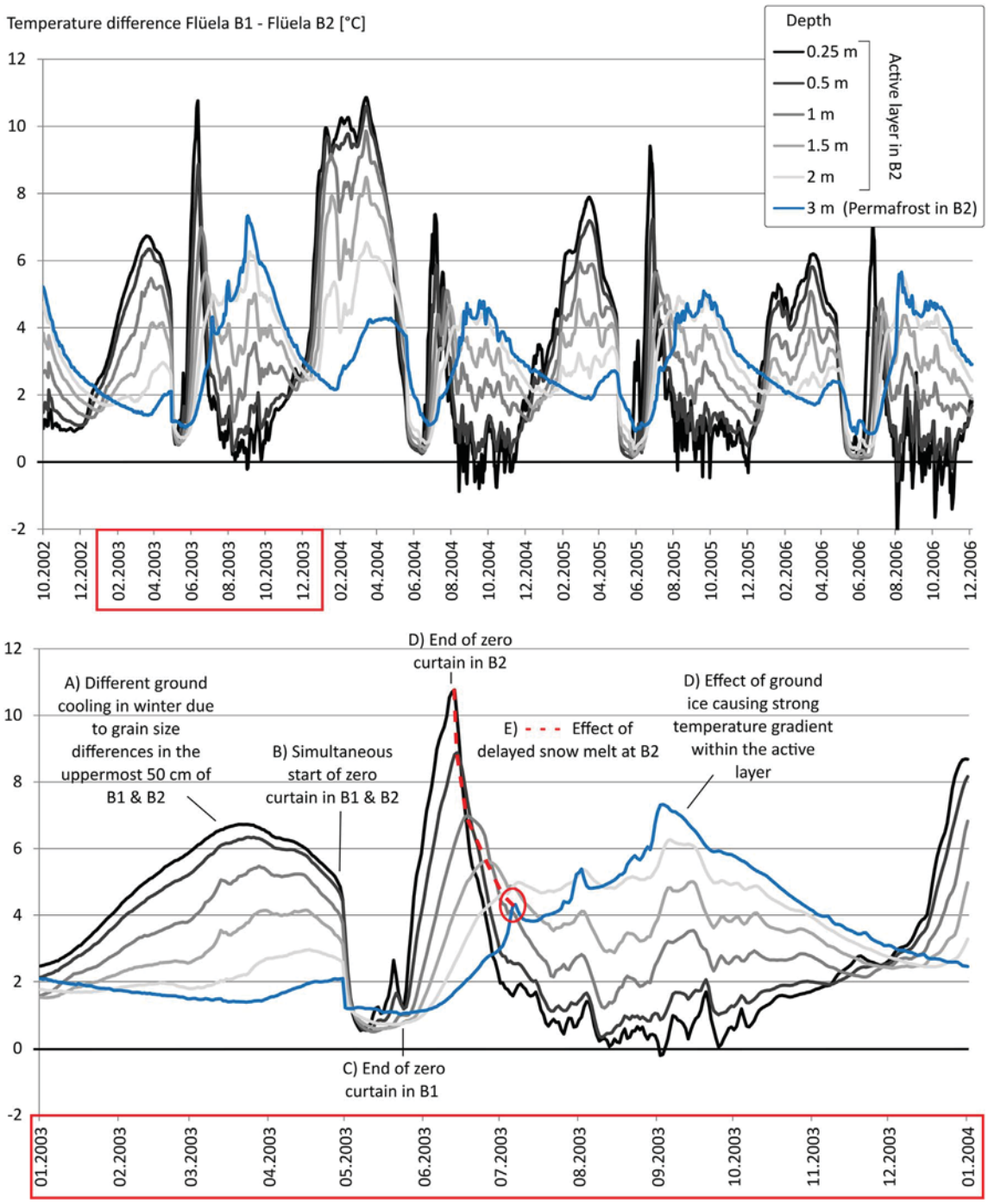

Fig. 11. Temperature differences between the boreholes B1 and B2 for different depths. Whereas temperatures differ strongest close to the surface in winter, the largest differences in summer occur at 3 m, close to the permafrost table in B2. The effect of different melt out dates is limited (Data: SLF/PERMOS).

frost) in the Mont Dolin talus slope adopted from Lambiel and Pieracci (2008) and areas with slope angles steeper than 30°. In contrast to a typical talus slope, the slope angle does not increase homogenously with elevation at this site. Accordingly, the ground ice distribution shows no typical "base of talus slope" pattern but follows the 30° slope limit.

5.2. The thermal influence of wind- or avalanche driven snow redistribution on permafrost in the Flüela talus slope

Former studies focused on the redistribution of snow as the explanation for the permafrost distribution at the Flüela site (Lerjen et al., 2003; Luetschg et al., 2004). The insulation theory focusses on snow redistribution by avalanches, causing ground cooling by long lasting or perennial snow deposits at the base of the slope, whereas areas above melt out earlier. Time-lapse images demonstrate that this typical melt out pattern does not occur every year (see for example Fig. 1). The date at which snow melt at B2 ends differs by up to 50 days within the 14 year time series we analysed (Table 1). Additionally there has no longer been any perennial snow as was documented by Haeberli (1975) for the early 1970s. Neither the interannual variation of the snow melt date, nor the long term changes regarding perennial snow patches have had a strong impact on AL thickness in B2, which has stayed very constant at circa 2.95 m for the entire time series. The limited sensitivity to interannual variations is typical for ice rich permafrost (Zenklusen Mutter and Phillips, 2012a), as is present at

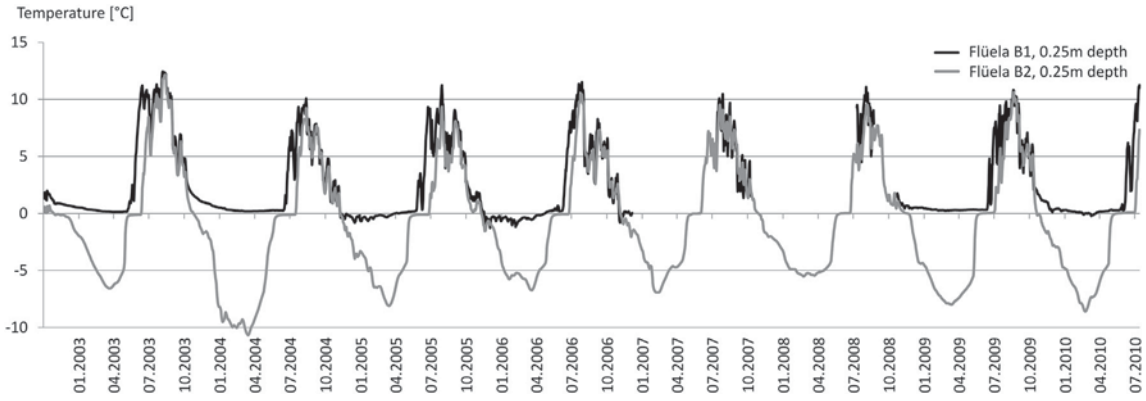

Fig. 12. Temperatures measured in B1 and B2 at 0.25 m depth. Whereas they are similar in summer, large differences are evident in winter and during snow melt. (Data: SLF/PERMOS).

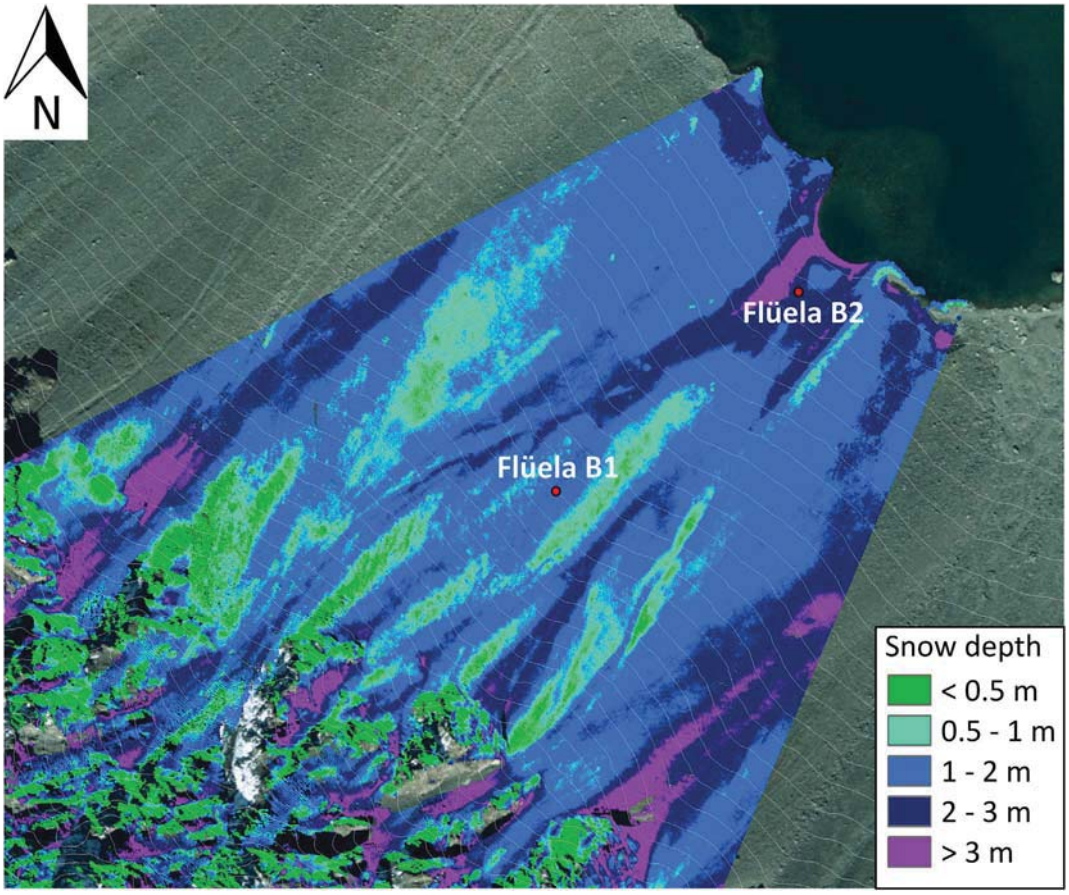

Fig. 13. Snow depths measured using terrestrial laser scanning in the Flüela talus slope on 23.01.2013. The borehole positions are shown.

B2 (Phillips et al., 2009, ERT results Fig. 9). If the insulation theory applies, long term changes in the date of snow melt should cause some reactions in permafrost.

A comparison of the temperatures in both boreholes might explain the absence of such reactions: the delay in snow melt at B2 has only a small effect on the ground temperatures near the permafrost table. Fig. 11 shows temperature differences between B1 and B2 for the AL and the uppermost permafrost thermistor in B2. The zero curtain during snow melt starts simultaneously in both boreholes but ends earlier in B1, which causes a steep peak in AL temperature differences. These peaks show a short delay with increasing depth but become considerably smaller towards the depth of permafrost in B2 (red dashed line in Fig. 11). If the duration of avalanche snow coverage were decisive for the thermal conditions in both boreholes, this peak should represent the maximum temperature difference between B1 and B2 at 2 or 3 m depth. According to the logic of the insulation theory, ground temperatures should converge again after the end of snow melt at B2. The temperatures continue to diverge, however, after this peak of snow melt (Fig. 11). The snow cover duration, thus, only has a subordinate effect on ground temperature in B2.

Furthermore, the insulation theory implies that the absence of permafrost in the upper talus slope should be caused by a stronger surface warming in summer because of the lack of insulation by avalanche snow. This effect, however, is rather small compared to the large differences in surface temperature regime between both boreholes in winter. Fig. 12 shows that ground temperatures at 0.25 m depth are quite similar in B1 and B2 after snowmelt in summer, but show differences of up to 10 °C during the whole winter season. Lerjen

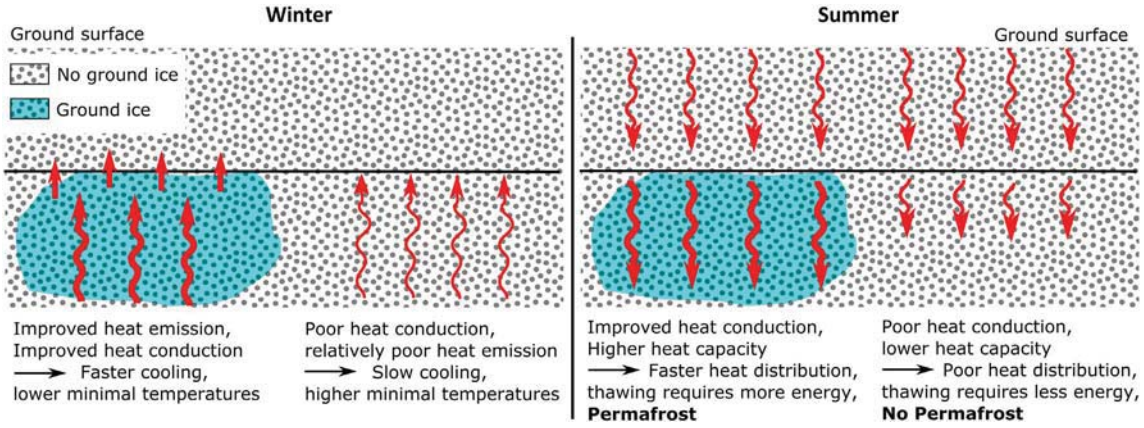

Fig. 14. Sketch showing the changes in the thermal characteristics of the ground caused by ground ice and how they contribute towards the presence of permafrost and its conservation.

et al. (2003) and Luetschg et al. (2004) supposed that winter snow erosion by wind contributes to these differences in winter ground cooling. A TLS survey from January 2013, however, shows much more snow already at the base of the talus slope where permafrost is present than in the upper permafrost-free parts (Fig. 13). We consider the snow distribution in Fig. 13 as being representative for early winter, because snow distribution patterns are particularly constant over the years, especially in pass regions (Mott et al., 2010). Wind driven snow erosion, therefore, does not seem to play a role for permafrost conservation. We hypothesize that the presence of permafrost is more likely influenced by the thermal characteristics of the ground than by snow redistribution.

5.3. The effect of soil/talus grain size and ground ice on the thermal characteristics of the ground

One explanation for the different ground surface cooling in winter in B1 and B2 is the difference in grain sizes and was described by all of the former studies at the Flüela site (Lerjen et al., 2003; Luetschg et al., 2004; Phillips et al., 2009). The upper 50 cm in borehole B1 consist of grass covered organic soils and sand, whereas coarse grained talus occurs at the surface at B2. As fine grained and vegetated soils have a higher water retention capacity, the water content can be higher and they cool down slower in autumn because of the release of latent heat during freezing (Schneider et al., 2012).

Coarse grained talus at the surface is also known to cause a cooling effect in summer (Gruber and Hoelzle, 2008; Schneider et al., 2012), however, this effect is not dominant here. In contrast to winter, the highest temperature differences in summer between B1 and B2 do not occur in the upper 0.5 m, which have different grain sizes - but they increase towards the depth of the permafrost in B2 (Fig. 11). This increase in temperature differences below 0.5 m depth occurs despite a very similar stratigraphy in both boreholes (Phillips et al., 2009). This implies that the thermal effect of the ground ice dominates the effect of the surface soil properties in summer and vice versa in winter.

Considering that permafrost is also absent in parts of the upper slope that have talus at the surface (Haeberli, 1975; Lerjen et al., 2003; Luetschg et al., 2004), the ground ice content appears to be the most relevant difference between both boreholes concerning the thermal regime. One common point of view is that perennial ground ice can develop because of permafrost conditions (Scapozza et al., 2011); this process was described by Haeberli and Vonder Mühll (1996) under the term congelation ice. We suggest that the opposite is also possible, i.e. that long term stable permafrost conditions can develop in a talus slope at or below the lower fringe of mountain permafrost because of the incorporation of snow or ice into the ground by mass wasting processes as explained in Section 5.1. This process of ground ice genesis is to a certain extent independent from the thermal ground conditions reigning at the time of deposition. As well as the soil grain sizes, the presence of ground ice, however, can change the thermal regime of the ground after its formation (Schneider et al., 2012).

Ice-rich permafrost is characterized by soil pore spaces that are completely filled or even oversaturated with ice (excess ice) (Ferrians, 1989). In contrast, ground devoid of ice contains air instead. The ice content increases the heat capacity of the ground, its thermal conductivity (Côté and Konrad, 2005) and its emissivity. In winter the high conductivity of ice saturated ground favours heat transfer upwards to the permafrost table and the heat emission towards the AL is faster. In summer energy is absorbed by the ice and rapidly distributed downward through the ice body, which is an efficient heat conductor. As long as the ice is not isothermal at 0 °C, it can absorb a large amount of energy without undergoing melt because of its high heat capacity in comparison to pore spaces filled with air (Fig. 14).

Ground ice acts as an effective heat sink: it rapidly absorbs and emits heat and distributes it over a larger area in ground. Incorporation of ice into the ground can, thus, allow the formation and conservation of permafrost in contrast to ice free ground, despite a similar energy budget at the surface. This implies that the thermally defined state of permafrost can be reached by the (non-thermal) process of ground ice formation.

6. Conclusions and implications for permafrost research

We postulate that the avalanche snow deposits located on permafrost ground at the foot of the Flüela talus slope indicate the formation of ice-rich frozen ground by burial and/or embedding of avalanche snow into coarse-grained debris, perhaps at times of more intense rock fall activity during the distant past (Late-glacial/early Holocene?). This process may have occurred in combination with insulation effects against radiation and atmospheric influences as earlier suggested by the insulation theory but could also have played a predominating role. The formation of ground ice initiated long-term thermally self-stabilising permafrost. Additional factors contributing to a contrasting thermal regime over the slope are the intra-talus ventilation and the different soil properties at the surface. The ventilation cools the ground below the permafrost and, thus, influences the lower edge of the permafrost body. The finer grained organic soil around B1 particularly reduces ground cooling in winter. The influence of these factors on the present day permafrost conditions, however, is limited: the ventilation only has a barely traceable effect on the permafrost temperatures and the permafrost distribution is not correlated with the presence of superficial talus.

Existing knowledge about the process of permafrost formation by mass movements, which probably dominates the lower belt of mountain permafrost is of particular relevance, because the coupling of these processes to climate change is not straightforward. Increases in rock fall activity induced by climate change might even favour the process of ground ice formation because of mass wasting processes. Paleoclimatic reconstructions related to permafrost and future permafrost distribution

modelling should carefully consider these aspects. Furthermore we conclude that:

- The effect of long lasting avalanche snow on ground temperature is indisputable but its effect on permafrost conservation is probably limited and may previously have been overestimated at the Flüela talus slope. Differences in surface heat exchange between B1 and B2, resulting from delayed snow melt at B2, have a relatively small influence on the temperatures close to the permafrost table. Strong temporal variabilities of the snow cover are neither reflected by the permafrost extent nor by the permafrost temperatures, at annual and multiannual scales.
- At the Flüelapass site, wind driven snow redistribution does not appear to influence the distribution of permafrost.
- The presence of a relict rock glacier at the lake bottom is additional proof of the existence of excess ice in the Flüela talus slope. The "Schottensee" lake at Flüelapass is younger than the relict subaquatic rock glacier and was dammed by a rock fall. Mega-ripples located below the rock fall deposit are an interesting indicator of a subsequent lake outburst.

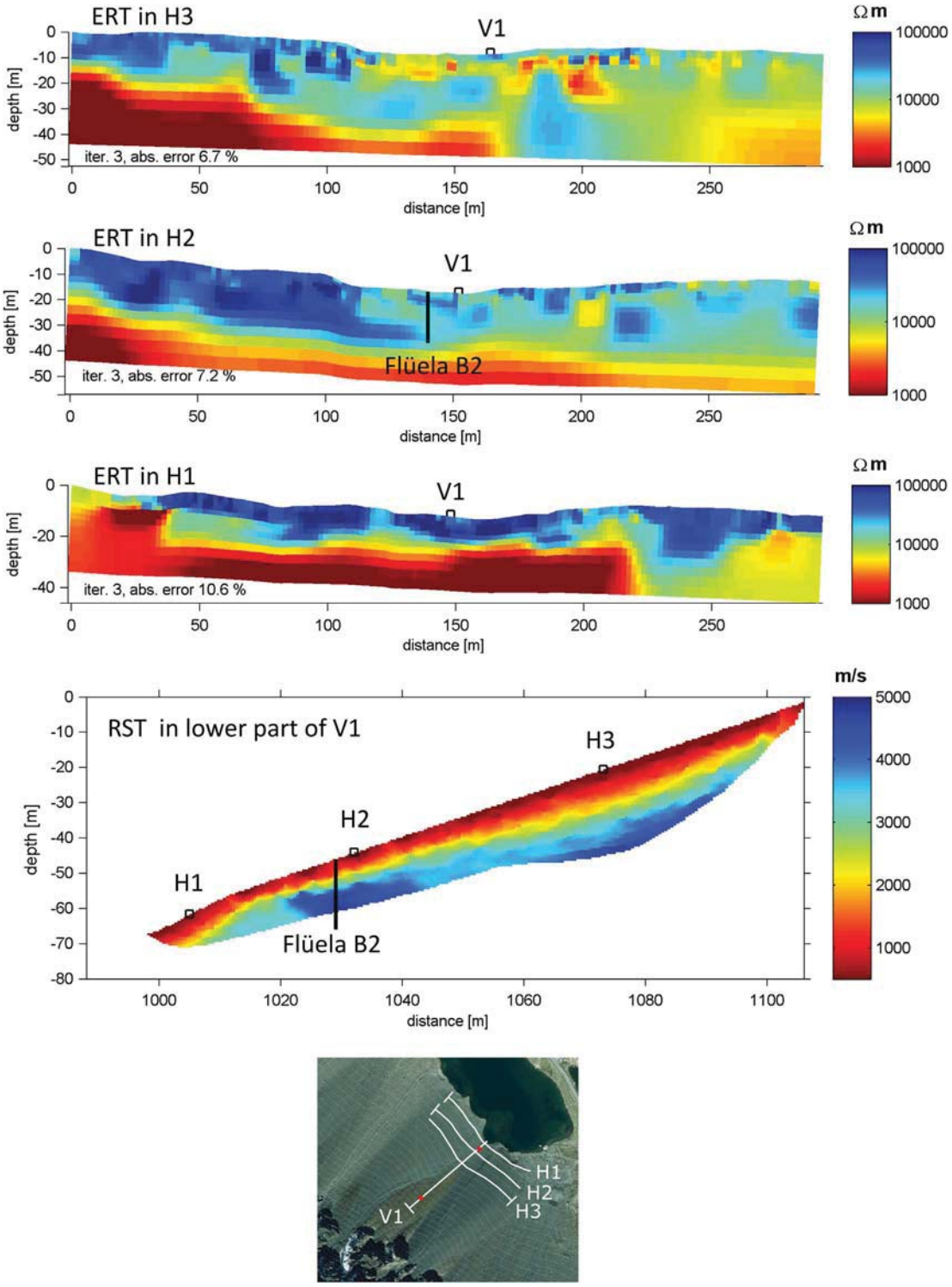

Fig. A. Horizontal ERT profiles and the vertical RST profile (bottom) acquired in the Flüela talus slope.

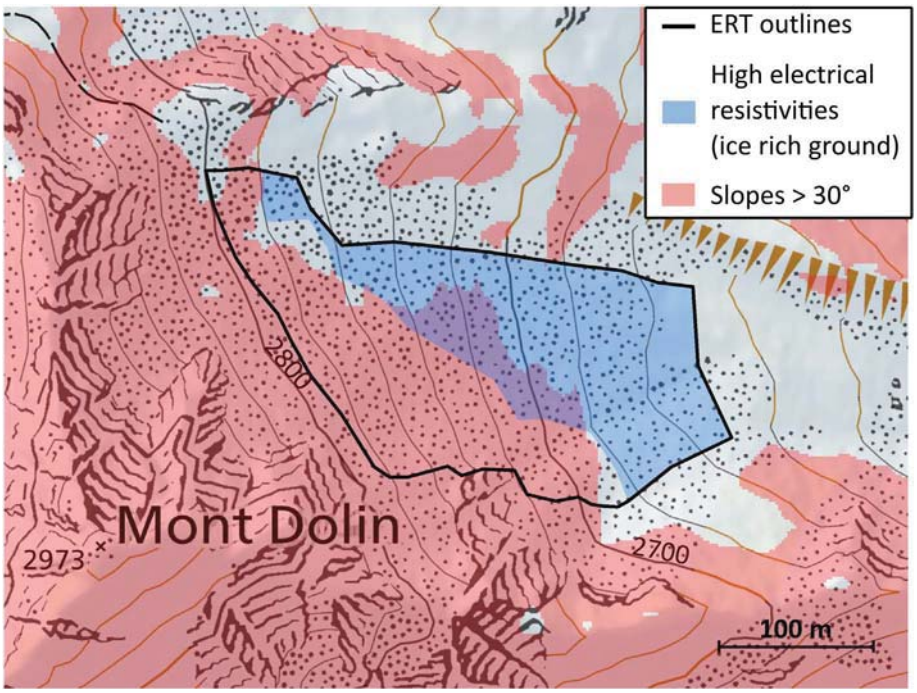

Fig. B. Adapted approximation of the ERT measurement results in Lambiel and Pieracci (2008) for the Mont Dolin talus slope in spatial comparison to areas with slope angles over 30°.

Acknowledgements

We kindly thank Martin Hiller (borehole electronics), Mark Schaer (subaquatic photography), Vali Meier (avalanche safety), Jürg Rocco (field observations) and all field assistants. The Flüelapass boreholes and geophysical data are part of PERMOS, the Swiss permafrost monitoring network. This study was partly funded by the SNF Sinergia project TEMPS (CRSII2_136279, 2011 – 2015) and by the Swiss Federal Office for the Environment FOEN. The Editor, an anonymous reviewer and particularly Wilfried Haeberli are warmly thanked for their useful comments and suggestions.

References

Arenson, L., Hoelzle, M., Springman, S., 2002. Borehole deformation measurements and internal structure of some rock glaciers in Switzerland. Permafr. Periglac. Process. 13, 117–135.

Ballantyne, C.K., 2002. Paraglacial geomorphology. Quat. Sci. Rev. 21 (18–19), 1935–2017.

Beltrami, H., 1996. Active layer distortion of thermal orbits. Permafr. Periglac. Process. 7, 101–110.

Boeckli, L., Brenning, A., Gruber, S., Noetzli, J., 2012. Permafrost distribution in the European Alps: calculation and evaluation of an index map and summary statistics. Cryosphere 6 (4), 807–820.

Bühler, Y., Adams, M.S., Bösch, R., Stoffel, A., 2016. Mapping snow depth in alpine terrain with unmanned aerial systems (UASs): potential and limitations. Cryosphere 10 (3), 1075–1088.

Burr, D.M., Baker, V.R., Carling, P.A., 2009. Megaflooding on Earth and Mars. Cambridge University Press.

Côté, J., Konrad, J.-M., 2005. A generalized thermal conductivity model for soils and construction materials. Can. Geotech. J. 42 (2), 443–458.

Delaloye, R., Lambiel, C., 2005. Evidences of winter ascending air circulation throughout talus slopes and rock glaciers situated in the lower belt of alpine discontinuous permafrost (Swiss Alps). Nor. Geogr. Tidsskr. 59, 194–201.

Etzelmüller, B., Hoelzle, M., Flo Heggem, E.S., Isaksen, K., Mittaz, C., Mühll, D.V., Ødegård, R.S., Haeberli, W., Sollid, J.L., 2001. Mapping and modelling the occurrence and distribution of mountain permafrost. Norsk Geografisk Tidsskrift - Norwegian Journal of Geography 55, 186–194.

Evatt, G.W., Abrahams, I.D., Heil, M., Mayer, C., Kingslake, J., Mitchell, S.L., Fowler, A.C., Clark, C.D., 2015. Glacial melt under a porous debris layer. J. Glaciol. 61 (229), 825–836.

Ferrians Jr., O.J., 1989. Glossary of permafrost and selected ground-ice terms. Can. Geotech. J. 26 (4), 769.

Fischer, L., Kääb, A., Huggel, C., Noetzli, J., 2006. Geology, glacier retreat and permafrost degradation as controlling factors of slope instabilities in a high-mountain rock wall: the Monte Rosa east face. Nat. Hazards Earth Syst. Sci. 6 (5), 761–772.

Frehner, M., Ling, A.H.M., Gärtner-Roer, I., 2015. Furrow-and-ridge morphology on Rockglaciers explained by gravity-driven buckle folding: a case study from the Murtèl Rockglacier (Switzerland). Permafr. Periglac. Process. 26 (1), 57–66.

Gądek, B., 2012. Debris slopes ventilation in the periglacial zone of the Tatra Mountains (Poland and Slovakia): the indicators. Cold Reg. Sci. Technol. 74–75, 1–10.

Gruber, S., Haeberli, W., 2007. Permafrost in steep bedrock slopes and its temperature-related destabilization following climate change. Journal of Geophysical Research: Earth Surface 112 (F2) (n/a-n/a).

Gruber, S., Haeberli, W., 2009. Mountain permafrost. In: Margesin, R. (Ed.), Permafrost Soils. Springer.

Gruber, S., Hoelzle, M., 2001. Statistical modelling of mountain permafrost distribution: local calibration and incorporation of remotely sensed data. Permafr. Periglac. Process. 12, 69–77.

Gruber, S., Hoelzle, M., 2008. The cooling effect of coarse blocks revisited: a modeling study of a purely conductive mechanism. In: Kane, D.L., Hinkel, K.M. (Eds.), 9th International Conference on Permafrost, Fairbanks, Alaska. University of Alaska Fairbanks, Institute of Northern Engineering, pp. 557–561.

Haeberli, W., 1975. Untersuchungen zur Verbreitung von Permafrost zwischen Flüelapass und Piz Grialetsch (Graubünden). Mitteilungen der Versuchsanstalt für Wasserbau, Hydrologie und Glaziologie der ETH Zürich, 17, Zurich (221 pp).

Haeberli, W., 1985. Creep of mountain permafrost: internal structure and flow of alpine rock glaciers. Mitteilung der VAW/ETH Zürich 77.

Haeberli, W., Vonder Mühll, D., 1996. On the Characteristics and Possible Origins of Ice in Rock Glacier Permafrost. Gebrüder Borntraeger, Stuttgart.

Haeberli, W., Hoelzle, M., Kääb, A., Keller, F., Vonder Mühll, D., Wagner, S., 1998. Ten years after drilling through the permafrost of the active rock glacier Murtèl, Eastern Swiss Alps: answered questions and new perspectives. In: A., G., L., A., Allard, M. (Eds.), Collection Nordicana, 7th International Conference on Permafrost, Yellowknife, Canada. Université Laval, Canada, pp. 403–410.

Haeberli, W., Kääb, A., Wagner, S., Vonder Mühll, D., Geissler, P., Haas, J.N., Glatzel-Mattheier, H., Wagenbach, D., 1999. Pollen analysis and ^{14}C age of moss remains in a permafrost core recovered from the active rock glacier Murtèl-Corvatsch, Swiss Alps: geomorphological and glaciological implications. J. Glaciol. 45 (149), 1–8.

Haeberli, W., Kääb, A., Vonder Mühll, D., Teysseire, P., 2001. Prevention of outburst floods from periglacial lakes at Grubengletscher, Valais, Swiss Alps. J. Glaciol. 47 (156), 111–122.

Haeberli, W., Hallet, B., Arenson, L., Elconin, R., Humlum, O., Kääb, A., Kaufmann, V., Ladanyi, B., Matsuoka, N., Springman, S., Vonder, Mühll D., 2006. Permafrost creep and rock glacier dynamics. Permafr. Periglac. Process. 17, 189–214.

Hauck, C., Kneisel, C., 2008. In: Hauck, C., Kneisel, C. (Eds.), Quantifying the ice content in low-altitude scree slopes using geophysical methods. Cambridge University Press, Applied Geophysics in Periglacial Environments, pp. 153–164.

Hilbich, C., 2010. Time-lapse refraction seismic tomography for the detection of ground ice degradation. Cryosphere 4, 243–259.

Hilbich, C., Fuss, C., Hauck, C., 2011. Automated time-lapse ERT for improved process analysis and monitoring of frozen ground. Permafr. Periglac. Process. 22 (4), 306–319. http://dx.doi.org/10.1002/ppp.732.

Humlum, O., Christiansen, H.H., Juliussen, H., 2007. Avalanche-derived rock glaciers in Svalbard. Permafr. Periglac. Process. 18 (1), 75–88.

Isaksen, K., Ødegård, R.S., Eiken, T., Sollid, J.L., 2000. Composition, flow and development of two tongue-shaped rock glaciers in the permafrost of Svalbard.

Permafr. Periglac. Process. 11 (3), 241–257.
Kääb, A., Reichmuth, T., 2005. Advance mechanisms of rock glaciers. Permafr. Periglac. Process. 16 (2), 187–193.
Kenner, R., Magnusson, J., 2017. Estimating the effect of different influencing factors on rock glacier development in two regions in the Swiss Alps. Permafr. Periglac. Process. 28 (1), 195–208.
Kenner R, Bühler Y, Delaloye R, Ginzler C, Phillips M. 2014. Monitoring of high alpine mass movements combining laser scanning with digital airborne photogrammetry. Geomorphology 206(0): 492–504.
King, L., Fisch, W., Haeberli, W., Waechter, H.P., 1987. Comparison of resistivity and radio-echo soundings on rock glacier permafrost. Z. Gletscherk. Glazialgeol. 23 (1), 77–97.
Kneisel, C., Hauck, C., 2003. Multi-method geophysical investigation of a sporadic permafrost occurrence. Z. Geomorph. N.F. 132, 145–159.
Kneisel, C., Schwindt, D., 2008. In: Kane, D.L., Kane, D.L., Kanes, D.L. (Eds.), Geophysical mapping of isolated permafrost lenses at a sporadic permafrost site at low altitude in the Swiss Alps, 9th International Conference on Permafrost, Fairbanks, Alaska. INE-UAF, pp. 959–964.
Lambiel, C., Pieracci, K., 2008. Permafrost distribution in talus slopes located within the alpine periglacial belt, Swiss Alps. Permafr. Periglac. Process. 19, 293–304.
Lerjen, M., Kääb, A., Hoelzle, M., Haeberli, W., 2003. Local distribution of discontinuous mountain permafrost. A process study at Flüela Pass, Swiss Alps. In: Phillips, M., Springman, S.M., Arenson, L.U. (Eds.), Eighth International Conference on Permafrost, Zurich. Swets & Zeitlinger, pp. 667–672.
Luethi, R., Phillips, M., 2016. Challenges and solutions for long-term permafrost borehole temperature monitoring and data interpretation. Geogr. Helv. 71 (2), 121–131.
Luetschg, M., Stoeckli, V., Lehning, M., Haeberli, W., Ammann, W., 2004. Temperatures in two boreholes at Flüela pass, eastern Swiss Alps: the effect of snow redistribution on permafrost distribution patterns in high mountain areas. Permafr. Periglac. Process. 15, 283–297.
Monnier, S., Kinnard, C., 2016. Interrogating the time and processes of development of the Las Liebres rock glacier, central Chilean Andes, using a numerical flow model. Earth Surf. Process. Landf. 41 (13), 1884–1893.
Morard, S., Delaloye, R., Lambiel, C., 2010. Pluriannual thermal behaviour of low elevation cold talus slopes in western Switzerland. Geographica Helvetica 65 (2), 124–134.
Mott, R., Schirmer, M., Bavay, M., Grünewald, T., Lehning, M., 2010. Understanding snow-transport processes shaping the mountain snow-cover. Cryosphere 4 (4), 545–559.
Mulsow, C., 2010. A flexible multi-media bundle approach. Int. Arch. Photogramm. Remote. Sens. Spat. Inf. Sci. 38, 472–477.
Munter, W., 2003. 3 × 3 Lawinen: Risikomanagement im Wintersport. Pohl & Schellhammer. (223 pp).
Nicholson, L., Benn, D.I., 2006. Calculating ice melt beneath a debris layer using meteorological data. J. Glaciol. 52 (178), 463–470.
Niu, F., Cheng, G., Niu, Y., Zhang, M., Luo, J., Lin, Z., 2016. A naturally-occurring 'cold earth' spot in Northern China. Scientific Reports 6, 34184.
Noetzli, J., Hoelzle, M., Haeberli, W., 2003. Mountain permafrost and recent Alpine rock-fall events: a GIS-based approach to determine critical factors. In: Phillips, M., Springman, S.M., Arenson, L.U. (Eds.), In, 8th International Conference on Permafrost, Zurich, Switzerland. Balkema, pp. 827–832.
Phillips, M., Zenklusen Mutter, E., Kern-Luetschg, M., Lehning, M., 2009. Rapid degradation of ground ice in a ventilated talus slope: Flüela Pass, Swiss Alps. Permafr. Periglac. Process. 20, 1–14.
Potter, J.N., 1972. Ice-cored rock glacier, Galena Creek, Northern Absaroka Mountains, Wyoming. Geol. Soc. Am. Bull. 83, 3025–3058.
Reznichenko, N., Davies, T., Shulmeister, J., McSaveney, M., 2010. Effects of debris on ice-surface melting rates: an experimental study. J. Glaciol. 56 (197), 384–394.
Rinner, K., 1969. Problems of two-medium-photogrammetry. Photogramm. Eng. 35 (2), 275–282.
Sanders, D., Widera, L., Ostermann, M., 2014. Two-layer scree/snow-avalanche triggered by rockfall (Eastern Alps): significance for sedimentology of scree slopes. Sedimentology 61 (4), 996–1030.
Sandmeier, K.J., 2014. REFLEXW—Software for the processing of seismic, acoustic or electromagnetic reflection, refraction and transmission data .
Sattler, K., Anderson, B., Mackintosh, A., Norton, K., de Róiste, M., 2016. Estimating permafrost distribution in the maritime southern alps, New Zealand, based on climatic conditions at rock glacier sites. Front. Earth Sci. 4 (4).
Scapozza, C., Lambiel, C., Baron, L., Marescot, L., Reynard, E., 2011. Internal structure and permafrost distribution in two alpine periglacial talus slopes, Valais, Swiss Alps. Geomorphology 132 (3–4), 208–221.
Schneider, S., Hoelzle, M., Hauck, C., 2012. Influence of surface and subsurface heterogeneity on observed borehole temperatures at a mountain permafrost site in the Upper Engadine, Swiss Alps. Cryosphere 6, 517–531.
Smerdon, J.E., Beltrami, H., Creelman, C., Stevens, M.B., 2009. Characterizing land surface processes: a quantitative analysis using air-ground thermal orbits. J. Geophys. Res. 114, D15102.
Springman, S.M., Arenson, L.U., Yamamoto, Y., Maurer, H., Kos, A., Buchli, T., Derungs, G., 2012. Multidisciplinary investigations on three rock glaciers in the Swiss Alps: legacies and future perspectives. Geografiska Annaler: Series A, Physical Geography 94, 215–243.
Suchlandt, O., Schmassmann, W., 1936. Limnologisehe Beobachtungen an acht Hochgebirgsseen der Landschaft Davos. Zeitschrift für Hydrologie 7, 1–2.
Wicky, J., Hauck, C., 2016. Numerical modelling of convective heat transport by air flow in permafrost-affected talus slopes. The Cryosphere Discuss. 2016, 1–29.
Zacharda, M., Gude, M., Vlastimil, R., 2007. Thermal regime of three low elevation scree slopes in Central Europe. Permafr. Periglac. Process. 18, 301–308.
Zenklusen Mutter, E., Phillips, M., 2012a. Active layer characteristics at ten borehole sites in Alpine permafrost terrain, Switzerland. Permafr. Periglac. Process. 23 (2), 138–151.
Zenklusen Mutter, E., Phillips, M., 2012b. Thermal evidence of recent talik formation in Ritigraben rock glacier: Swiss Alps. In: Hinkel, M. (Ed.), 10th International Conference on Permafrost, Salekhard, Russia. The Northern Publisher, pp. 479–483.